nature structural & molecular biology

MIA40 is an oxidoreductase that catalyzes oxidative protein folding in mitochondria

Lucia Banci[1,2], Ivano Bertini[1,2], Chiara Cefaro[1,2], Simone Ciofi-Baffoni[1,2], Angelo Gallo[1,2], Manuele Martinelli[1,2], Dionisia P Sideris[3,4], Nitsa Katrakili[3] & Kostas Tokatlidis[3,5]

MIA40 has a key role in oxidative protein folding in the mitochondrial intermembrane space. We present the solution structure of human MIA40 and its mechanism as a catalyst of oxidative folding. MIA40 has a 66-residue folded domain made of an α-helical hairpin core stabilized by two structural disulfides and a rigid N-terminal lid, with a characteristic CPC motif that can donate its disulfide bond to substrates. The CPC active site is solvent-accessible and sits adjacent to a hydrophobic cleft. Its second cysteine (Cys55) is essential *in vivo* and is crucial for mixed disulfide formation with the substrate. The hydrophobic cleft functions as a substrate binding domain, and mutations of this domain are lethal *in vivo* and abrogate binding *in vitro*. MIA40 represents a thioredoxin-unrelated, minimal oxidoreductase, with a facile CPC redox active site that ensures its catalytic function in oxidative folding in mitochondria.

Disulfide bonds are crucial for maintaining the structural stability of proteins and are involved in various redox-signaling pathways in cells. The introduction of disulfide bonds *in vivo* often requires the coordinated action of dedicated enzymes that act as catalysts for the oxidative folding process necessary to adopt a native conformation. Most of our understanding about oxidative folding pathways comes from studies on the eukaryotic protein disulfide isomerase (PDI), which resides in the lumen of the endoplasmic reticulum (ER)[1–3], and on the bacterial periplasmic disulfide bond (Dsb) proteins[4–6]. Recently, a similar process of oxidative folding has been discovered to operate in the mitochondria of eukaryotic cells[7–10]. Several cysteine-rich proteins of the mitochondrial intermembrane space (IMS) were found to undergo oxidation after entering the organelle, in a pathway that requires the proteins Mia40 and Erv1 and is ultimately linked to the respiratory chain[9,11–14].

Mia40 belongs to a protein family whose members share six completely conserved cysteine residues constituting a -CPC-CX_9C-CX_9C- motif[7,15,16]. Mia40 primary sequences can, however, vary substantially in length. The human homolog (MIA40, 142 residues) shares high sequence identity (>50%) with its eukaryotic homologs in the central part of its sequence (residues 47–105), which includes the conserved -CPC-CX_9C-CX_9C- motif (**Fig. 1a**). Outside this region, the level of homology between different species is low (<20%). MIA40 lacks a large N-terminal extension including a transmembrane region with respect to the yeast homologs (**Fig. 1a**), thus being completely soluble in the IMS[17]. Substrate proteins for Mia40 are IMS proteins of less than 20 kDa containing characteristic cysteine motifs, organized in twin CX_3C, twin CX_9C or CX_2C motifs[18]. Among them is the mitochondrial copper chaperone Cox17 (a CX_9C substrate), which participates in Cu(I) transfer to cytochrome *c* oxidase (CcO)[19–21], and the small Tims (CX_3C substrates), which are chaperones for mitochondrial membrane proteins[22–24]. The Mia40-based protein-import mechanism is therefore vital to allow a correct function of several mitochondrial processes such as respiration and protein biogenesis.

On the basis of binding experiments *in vitro* and *in organello*, it has been proposed that Mia40 introduces disulfide bonds into imported precursor substrates after they cross the outer membrane protein-import channel[7,9]. In a cascade of oxidoreductase reactions, electrons are then transferred from Mia40 to Erv1 and finally to either oxygen or cytochrome *c*[11–13]. Such a pathway resembles the reaction cascades underpinning the oxidative folding process in the ER and bacterial periplasm, involving Ero1–Erv2–PDI and DsbB–DsbA, respectively[4,5,25–27]. The identification of transient intermolecular disulfide bonds (mixed disulfides) between Erv1 and Mia40, as well as between Mia40 and its substrate proteins, such as Cox17 and Tim proteins, supports the model of a regulated transfer of disulfide bonds[7,9,14,28–30]. However, direct molecular evidence on the mechanism of Mia40-dependent oxidation of the substrates and the structural basis of this process are lacking.

Here we reveal the molecular mechanism of Mia40-dependent oxidative folding. This was achieved through structural characterization

[1]Magnetic Resonance Center CERM, University of Florence, Via Luigi Sacconi 6, 50019, Sesto Fiorentino, Florence, Italy. [2]Department of Chemistry, University of Florence, Via della Lastruccia 3, 50019 Sesto Fiorentino, Florence, Italy. [3]Institute of Molecular Biology and Biotechnology, Foundation for Research and Technology Hellas (IMBB-FORTH), Heraklion 71110, Crete, Greece. [4]Department of Biology, University of Crete, Heraklion 71409, Crete, Greece. [5]Department of Materials Science and Technology, University of Crete, Heraklion 71003, Crete, Greece. Correspondence should be addressed to I.B. (bertini@cerm.unifi.it) or K.T. (tokatlid@imbb.forth.gr).

Received 27 May 2008; accepted 5 January 2009; published online 1 February 2009; doi:10.1038/nsmb.1553

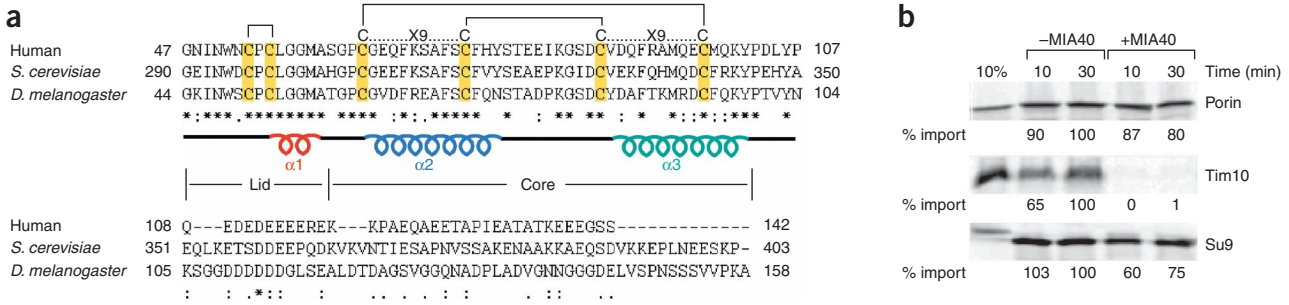

Figure 1 MIA40 is functionally active in binding substrates. (**a**) Sequence alignments of Mia40 orthologs. The protein secondary structure based on chemical shift index analysis of MIA40 is reported below the alignment. The N-termimal lid and the α-hairpin core are indicated (see text for details). Helices α1 (red), α2 (blue) and α3 (cyan) are shown. The conserved cysteine motif CPC and twin CX_9C motifs are shown in yellow; intramolecular disulfide pairings (determined here) are shown above the alignment. (**b**) Competition import assays. ^{35}S-labeled Porin, Tim10 and Su9-DHFR from yeast were mixed with or without MIA40 and imported into yeast mitochondria at 30 °C for the indicated time points. The imported material was analyzed by reducing SDS-PAGE, visualized by autoradiography and quantified as a percentage imported relative to the starting amount.

of MIA40 and investigation *in vitro* and *in vivo* of its interaction with COX17 and Tim substrates. The CPC motif is the active site of MIA40, rapidly catalyzing the formation of a disulfide bond in the substrates.

RESULTS

MIA40 binds substrates as a monomer *in vitro*

MIA40 purified from *Escherichia coli* cells (**Supplementary Methods** online) is functionally active, as assessed by testing its binding ability to an authentic substrate (Tim10) or to two control proteins (outer membrane porin and matrix-targeted Su9-DHFR) using import-competition assays (**Fig. 1b**). Such an assay was used previously to test the functionality of the TIM10 complex in binding its cognate import substrate[31]. Radiolabeled precursor proteins (Tim10, porin or Su9-DHFR) were incubated with MIA40 purified in aerobic conditions—that is, in its fully oxidized state—and then with isolated mitochondria. MIA40 inhibited specifically the import of Tim10 by more than 99% but only weakly that of porin or Su9-DHFR (**Fig. 1b**). MIA40 directly bound radiolabeled Tim10, because a β-mercaptoethanol–sensitive mixed disulfide intermediate was detected. Additionally, MIA40 is monomeric *in vitro*, as shown by static multiangle light scattering and confirmed by a correlation time for the molecule tumbling (τ_m), of 10.6 ± 0.5 ns from NMR heteronuclear relaxation data (**Supplementary Fig. 1** online).

^{13}C NMR reveals distinct redox properties of MIA40 disulfides

NMR Cβ chemical shifts are characteristic of the oxidation state of cysteines[32]. In aerobic conditions as purified from bacterial cell cultures, the six conserved cysteine residues of MIA40 (-CPC-CX_9C-CX_9C-) are engaged in three disulfide bonds ($MIA40_{3S\text{-}S}$). The CPC (Cys53-Pro54-Cys55) motif could be easily reduced by a low concentration of DTT (2 mM) (**Fig. 2**). Reduction of the CPC motif entails only local structural changes for the segment 50–64, which encompasses the N-terminal lid domain, as shown by ^{1}H- and ^{15}N chemical shift changes (**Fig. 2a**,**b**). In contrast, no chemical shift variations were detected for the residues of the 'core' domain (**Fig. 2a**,**b**), even after treatment with 100 mM DTT (**Supplementary Fig. 2** online), indicating that the CX_9C disulfides were still in an oxidized state. This behavior was confirmed by AMS (4-acetamido-4′-maleimidylstilbene-2,2′-disulfonic acid) thiol trapping assays (**Supplementary Fig. 2** and **Supplementary Methods**). These data, in agreement with a previous biochemical study[33], provide a structural basis for the observed redox behavior of MIA40.

The reduction potential of the easily reducible CPC motif in the redox couple $MIA40_{3S\text{-}S}$–$MIA40_{2S\text{-}S}$, is −200 ± 5 mV, as measured by fluorescence emission spectra (**Fig. 3a**,**b**). This value of redox potential lies between those of Mia40 substrates (for example, −340 mV for COX17 and −320 mV for yeast Tim10) and the enzymatic C-terminal intramolecular cysteine pair C130-C133 of yeast Erv1 (−150 mV[13]; **Fig. 3c**). Therefore, on thermodynamic grounds alone, these values support the disulfide-relay reactions observed in mitochondria where reducing equivalents flow from the substrate to the CPC motif of Mia40 and then to Erv1.

Solution structure defines MIA40 as a new type of oxidoreductase

Chemical shift index analysis[34] indicates that both $MIA40_{3S\text{-}S}$ and $MIA40_{2S\text{-}S}$ states have a small helical segment in residues 56–59 (helix α1) and two longer helical segments (helix α2, residues 65–77, and helix α3, residues 88–100), whereas the other 80% of residues, essentially located at the N and C termini, do not take any secondary-structural conformation (**Fig. 4a**), a large part of them being highly flexible. Regions 1–41 and 107–142 indeed have R_2/R_1 ratios below those of the α-helical regions (**Supplementary Fig. 1**) and are characterized by negative or low (<0.5) ^{15}N{^{1}H} NOE values (**Fig. 4b**). By contrast, the region containing the CX_9C motifs, as well as that encompassing the N-terminal helix α1, have R_2/R_1 (**Supplementary Fig. 1**) and ^{15}N{^{1}H} NOE values consistent with a structured conformation (**Fig. 4b**). The unstructured C terminus is not essential *in vivo*, as a yeast Mia40 mutant lacking this C-terminal segment could support growth to wild-type levels (data not shown). Similarly, it was previously shown that the N-terminal segment is dispensable for function[33].

The solution structure of the folded central region of $MIA40_{2S\text{-}S}$, determined by NMR (**Fig. 5a** and **Supplementary Fig. 3** online), consists of a 'core' and a 'lid' on top of it. The core is composed of helices α2 (residues 65–77) and α3 (residues 88–100), which form an antiparallel α-hairpin kept together by two disulfide pairs, Cys64-Cys97 and Cys74-Cys87, juxtaposing the CX_9C motifs (**Fig. 5a**). The lid (residues 41–64) folds onto the core and is structurally rigid, although it does not have defined secondary-structural elements, with the exception of the short helix α1 (residues 56–59; **Fig. 5a**). The two residues preceding the lid segment, Pro54 and Cys55, also show some α-helical propensity (~40% of 30 energy-minimized structures). However, the disappearance of the NH signal of Cys55 in $MIA40_{2S\text{-}S}$ indicates local structural flexibility in the CPC region. In contrast, this

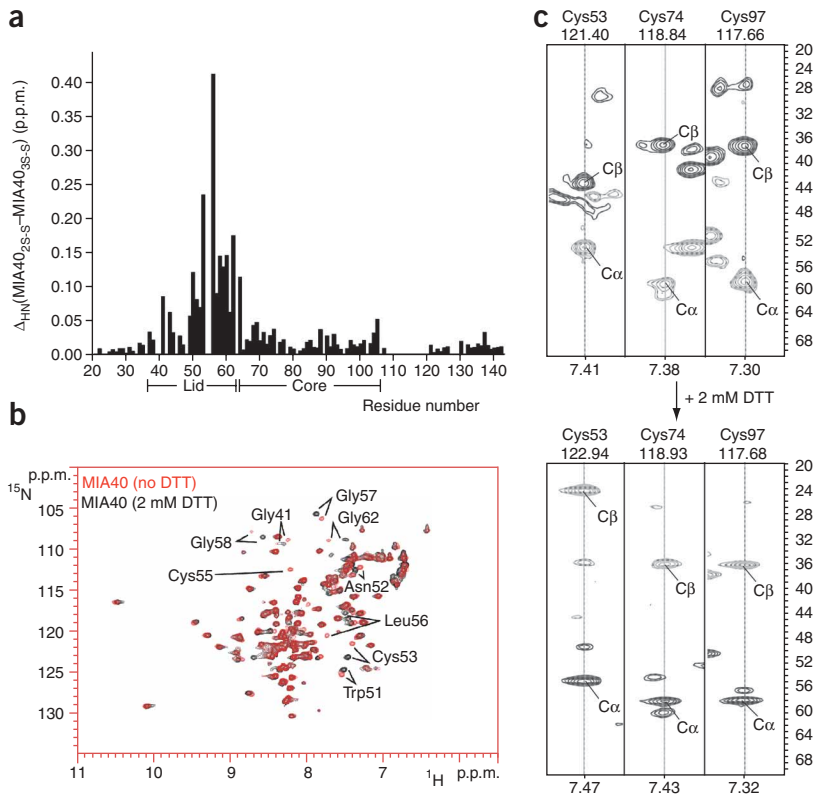

Figure 2 The redox and structural properties of the CPC intramolecular disulfide bonds of human MIA40. (**a**) The weighted-average chemical shift differences Δ_{HN} (that is, $([(\Delta H)^2 + (\Delta N / 5)^2] / 2)^{1/2}$, where ΔH and ΔN are chemical shift differences for ^1H and ^{15}N, respectively) between MIA40$_{2S-S}$ and MIA40$_{3S-S}$. (**b**) Superimposition of two-dimensional ^1H-^{15}N HSQC spectra (800 MHz, 298 K) of MIA40$_{2S-S}$ (black) and of MIA40$_{3S-S}$ (red). Residues with NH chemical shifts that change upon reduction lie in the vicinity of the CPC motif (indicated in the NMR spectra). (**c**) Cβ and Cα chemical shift values of Cys53, Cys74 and Cys97, either involved or not involved in disulfide bonds with Cys55, Cys87 and Cys64, respectively, are shown in the CBCANH NMR experiment in the absence and in the presence of 2 mM DTT.

NH signal is still detectable in MIA40$_{3S-S}$, suggesting an increased structural rigidity upon disulfide-bond formation. The difference in backbone flexibility between the two redox states of MIA40 may have a role in the catalytic process.

Notably, the lid contains conserved hydrophobic residues that interact with conserved aromatic residues located on one side of the α-hairpin core. Indeed, a highly charged region is only present on the α-hairpin face opposite the CPC motif (**Fig. 5b**). The hydrophobic interactions between the lid and the α-hairpin core position the CPC motif in a solvent-exposed conformation protruding from a hydrophobic cleft (**Fig. 5c**, red), which consists of the strictly conserved phenylalanine residues Phe68, Phe72, Phe75 and Phe91, as well as Leu42, Ile43, Ile49, Trp51, Leu56, Met59, Ala60, Met94 and Met98 (**Fig. 5d**). The second cysteine, Cys55, of the CPC motif (**Fig. 5c**,**d**, yellow) lies directly above this characteristic hydrophobic cleft.

In summary, the salient structural features of MIA40 are (i) a high proportion of unfolded segments at the N and C termini, (ii) a folded α-hairpin core stabilized by structural disulfide pairings, (iii) a rigid N-terminal lid with an extensive array of hydrophobic interactions with one part of the α-hairpin core and (iv) a solvent-exposed CPC motif ideally placed to be the active site in the oxidation process, with its second cysteine, Cys55, lying adjacent to a hydrophobic cleft that may function as a substrate binding site.

The electron-transfer mechanism of MIA40-catalyzed oxidative folding

Spontaneous air oxidation in the absence of MIA40 can oxidize only ~10% of fully reduced COX17$_{6SH}$ to the partially oxidized COX17$_{2S-S}$ form (with two disulfide pairs created between the twin CX_9C motifs of Cox17) in 12 h. By contrast, MIA40$_{3S-S}$ can quantitatively and rapidly (less than 30 min) oxidize COX17$_{6SH}$ to COX17$_{2S-S}$, as monitored through ^1H-^{15}N NMR spectra (**Fig. 6a**). These spectra show that, upon addition of MIA40$_{3S-S}$, the NH resonance pattern of COX17$_{6SH}$ drastically changes to that of COX17$_{2S-S}$—that is, the form

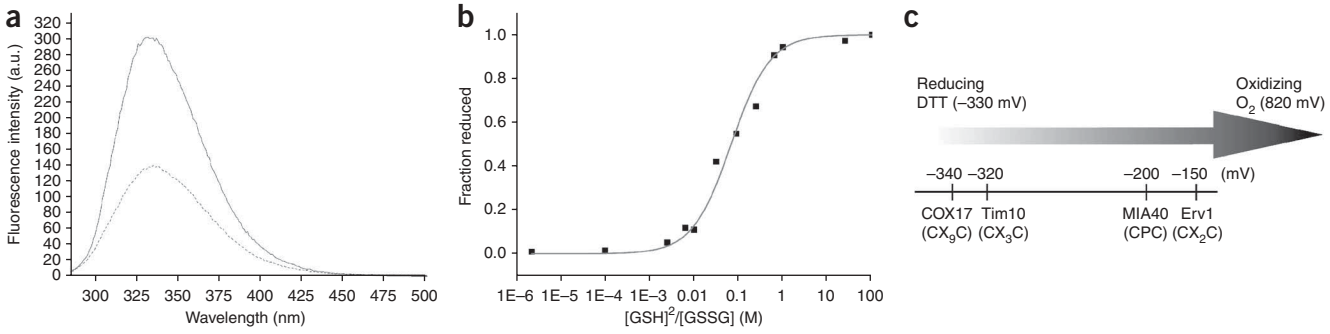

Figure 3 Redox potential of the CPC redox active site. (**a**) Fluorescence emission spectra of the oxidized (50 mM phosphate buffer, pH 7.0, 0.01 mM GSSG; broken line) and the reduced (50 mM phosphate buffer, pH 7.0, 200 mM GSH; solid line) MIA40 after excitation at 280 nm. (**b**) The redox equilibrium of MIA40 with different $[GSH]^2$/GSSG ratios is shown. Data processing and determination of the equilibrium constant are previously described[51]. After nonlinear regression, a value of K_{eq} = 68.4 mM ± 7.9 (correlation coefficient: 0.987) was obtained for the MIA40/glutathione equilibrium, corresponding to a redox potential of −200 ± 5 mV for the MIA40$_{3S-S}$–MIA40$_{2S-S}$ redox couple. (**c**) Comparison of the redox potential of MIA40 to that of components of the disulfide relay system in the IMS.

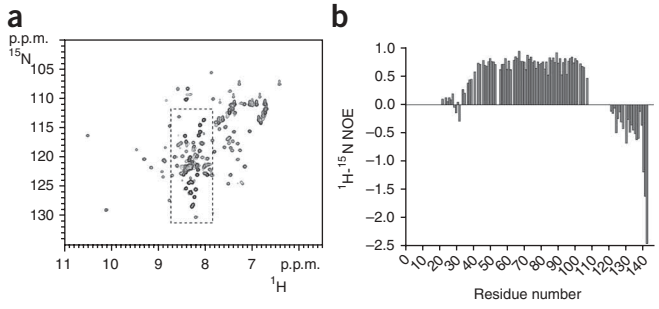

Figure 4 MIA40 is substantially unstructured at its N and C termini. (**a**) ^{1}H-^{15}N HSQC spectrum of MIA40$_{2S\text{-}S}$ showing that NH signals clustered in the central region (bordered by a broken line) belong mainly to the unstructured N and C termini of the protein. (**b**) ^{15}N{^{1}H} NOE versus MIA40$_{2S\text{-}S}$ residue number collected at 600 MHz in 50 mM phosphate buffer, pH 7, and 2mM DTT. Reliable relaxation values cannot be obtained for residues 109–118 as their NH cross-peaks are overlapped in the NMR spectra.

where Cys25, Cys35, Cys44 and Cys54 are oxidized—while the copper binding Cys22 and Cys23 ligands remain in a reduced state and therefore do not participate in the electron-transfer reaction. Consistent with this observation, MIA40$_{3S\text{-}S}$ undergoes reduction to MIA40$_{2S\text{-}S}$ (**Fig. 6a**). Clear NH resonance changes are seen for Cys53 and Cys55 of the CPC motif of MIA40, but also for some neighboring residues (Trp51, Asn52, Gly62, Gly57 and Gly58, indicated in **Figure 6a**) that are all part of the N-terminal lid. Upon titration of ^{15}N-labeled MIA40$_{3S\text{-}S}$ with increasing amounts of ^{15}N-labeled COX17$_{6SH}$, the MIA40$_{3S\text{-}S}$ signal intensity seemed to decrease with increasing COX17$_{6SH}$ concentration and, concomitantly, the signals corresponding to MIA40$_{2S\text{-}S}$ and COX17$_{2S\text{-}S}$ appeared and increased in intensity, with the reaction being complete at 1:1 protein:protein ratio (**Fig. 6b**,**c**).

Considering that two disulfides in COX17$_{2S\text{-}S}$ are formed to the detriment of one in MIA40$_{3S\text{-}S}$ and that oxygen is difficult to eliminate from our reaction mixture, we postulate that the second disulfide pairing in COX17 is mediated by oxygen. As there are two electrons involved in the latter reaction, we guessed that transient H_2O_2 was formed, and we could indeed detect it through a colorimetric H_2O_2 assay. However, the formation of the first disulfide bond, which is MIA40$_{3S\text{-}S}$ dependent, is a prerequisite for substrate oxidation, as upon addition of MIA40$_{2S\text{-}S}$ (where oxygen is still present) to COX$_{6SH}$ no electron transfer was observed. To define which is the crucial disulfide bond of COX17 formed by MIA40, we produced two mutants of COX17 (CX$_9$S/SX$_9$C and SX$_9$C/CX$_9$S) with ^{15}N,^{13}C-selectively labeled cysteine residues and used NMR to investigate their reactions with MIA40$_{3S\text{-}S}$. Disulfide-bond formation between the two remaining cysteine residues of CX$_9$C motifs was detected only in the presence of the SX$_9$C/CX$_9$S mutant (**Fig. 6d**). This result was supported by import experiments in isolated mitochondria where the mixed intermediate with MIA40 could still form substantially for the SX$_9$C/CX$_9$S (or C1/4S) mutant but was almost entirely abolished for the CX$_9$S/SX$_9$C (or C2/3S) mutant (**Fig. 6e**). Therefore, MIA40$_{3S\text{-}S}$ specifically catalyzes the formation of the inner disulfide bond between Cys35 and Cys44 in COX17.

We found that the same reaction features occur in intact mitochondria, where the crucial mixed disulfide intermediate of the oxidative folding reaction could be trapped and monitored (**Fig. 7a**). COX17 was imported efficiently into isolated yeast mitochondria, where it forms a transient mixed disulfide intermediate with endogenous Mia40 within 2 min of import (shown by a blue arrowhead in **Figure 7a**). The intermediate was stabilized by *N*-ethyl-maleimide (NEM) treatment, which blocks unreacted cysteines, thereby arresting the substrate in transit and bound to Mia40 (ref. 30). Imported COX17 (initially mostly in a reduced state, shown in green) became gradually oxidized (shown in brown) to the detriment of the mixed disulfide species (shown in blue), which disappears, as would be expected for a productive intermediate (**Fig. 7b**).

We further dissected the functional role of the cysteines in the CPC motif by investigating the impact of cysteine mutations *in vivo* using yeast cells, and *in vitro* using a reconstituted system. We generated three mutants of the CPC motif (SPS, CPS and SPC, exchanging the corresponding cysteine with serine) and tested them in complementation assays with a *GALMia40* strain, which grows well on galactose (SG↑) but not on glucose (SC↓) or lactate (SL↓) (**Fig. 7c**, above, 'Empty', and **Supplementary Methods**). When *GALMia40* cells were transformed with a plasmid carrying wild-type yeast *Mia40*, their growth was restored on glucose and lactate (**Fig. 7c**, middle, 'WT'). However, the CPS and SPS mutations were lethal,

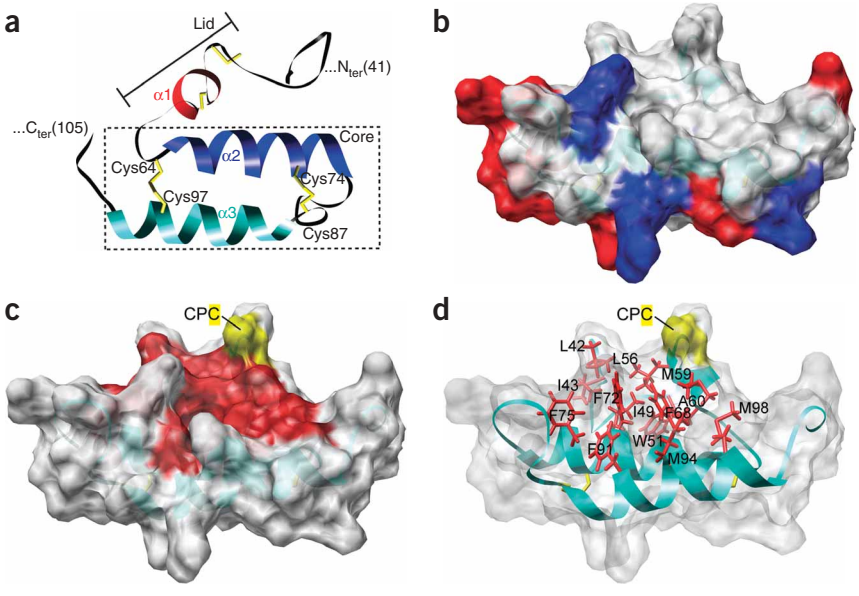

Figure 5 The solution structure of MIA40$_{2S\text{-}S}$. (**a**) Ribbon diagram of the lowest-energy conformer of MIA40$_{2S\text{-}S}$. Helix α1 of the N-terminal lid is shown in red, and helices α2 and α3 composing the α-hairpin core are shown in blue and cyan. Disulfide pairings (or free thiols) are shown in yellow. (**b**) Surface representation of MIA40$_{2S\text{-}S}$, mapping the electrostatic potential. White, uncharged residues; red, acidic residues; blue, basic residues. (**c**) The hydrophobic cleft on the surface of MIA40$_{2S\text{-}S}$ is shown in red, with ribbon diagram in transparent cyan. The second cysteine of the CPC motif, Cys55, which lies adjacent to the hydrophobic cleft, is shown in yellow. (**d**) The conserved residues making up the hydrophobic cleft on the surface of MIA40$_{2S\text{-}S}$ are annotated and shown in red. The ribbon diagram is shown in transparent cyan and Cys55 is shown in yellow.

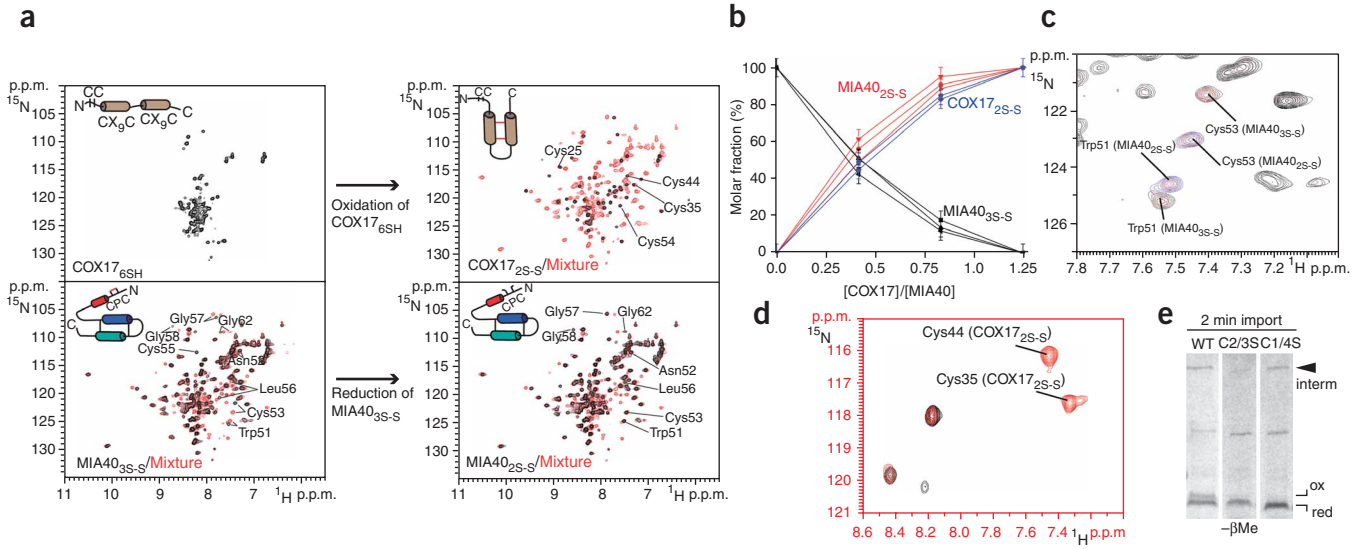

Figure 6 Interaction of MIA40 with substrates. (**a**) Oxidation and reduction processes of $COX17_{6SH}$ and $MIA40_{3S\text{-}S}$, respectively, as followed by NMR. The ^{1}H-^{15}N HSQC spectrum of a 1:1 ^{15}N-labeled $MIA40_{3S\text{-}S}$ / ^{15}N-labeled $COX17_{6SH}$ mixture is superimposed with the ^{1}H-^{15}N HSQC spectra of $MIA40_{3S\text{-}S}$ or $MIA40_{2S\text{-}S}$ or $COX17_{2S\text{-}S}$. The ^{1}H-^{15}N HSQC spectrum of $COX17_{6SH}$ is also shown. NH resonances of cysteine residues and some surrounding residues of MIA40 and COX17 are indicated in the NMR spectra. The disulfide formation in COX17 (above) and disruption in MIA40 (below) in relation to their structural changes are shown schematically in the inset. (**b**) Plot shows the formation of $MIA40_{2S\text{-}S}$ (red) and $COX17_{2S\text{-}S}$ (blue) and the decrease in of $MIA40_{3S\text{-}S}$ level (black) as a function of the COX17 / MIA40 molar ratio. The cross-peaks of residues Trp51, Cys53 and Gly57, whose ^{1}H- and ^{15}N chemical shifts change substantially depending on the redox state of MIA40, have been selected to evaluate the molar fraction of MIA40, whereas those of residues Lys44 and Glu47 provide the molar fraction of $COX17_{2S\text{-}S}$. (**c**) Overlay of a selected region of the ^{1}H-^{15}N HSQC spectra of $MIA40_{3S\text{-}S}$ in the presence of 0 (black), 0.5 (red) or 1.2 (blue) equivalents of ^{15}N-labeled $COX17_{6SH}$, showing the quantitative formation of $MIA40_{2S\text{-}S}$ at a 1:1 protein ratio. (**d**) Overlay of the ^{1}H-^{15}N HSQC spectra of the (^{13}C,^{15}N)Cys-selectively labeled SX_9C/CX_9S $COX17_{6SH}$ mutant in the presence of 0 (black) and 1 (red) equivalents of unlabeled $MIA40_{3S\text{-}S}$, showing the formation of NH cross-peaks with ^{1}H- and ^{15}N chemical shifts typical of those found for Cys44 and Cys35 in wild-type $COX17_{2S\text{-}S}$. (**e**) ^{35}S-labeled COX17 and the cysteine-to-serine mutants C1/4S (outer disulfide bridge) or C2/3S (inner disulfide bridge) were imported into wild-type (WT) yeast mitochondria for 2 min at 30 °C, followed by nonreducing SDS-PAGE and autoradiography. The mixed disulfide intermediate (interm) with yeast Mia40 is shown with an arrowhead, and the oxidized (ox) and reduced (red) species of COX17 are indicated.

supporting the concept that the second cysteine of the CPC motif is crucial for survival of the cells. The SPC mutant survived, but had a clear growth defect compared to the wild type. The viability of the SPC mutant can be explained by the fact that this mutant protein has a high tendency to form intermolecular disulfide-bonded dimers *in vitro* (**Supplementary Fig. 4** online) and that it is trapped in a DTT-sensitive high-molecular-weight complex *in vivo* (data not shown). Thus, this intermolecular disulfide bond can act as the catalytic site.

In an *in vitro* reconstituted system, bead-immobilized yeast Mia40 was previously reported to efficiently bind substrates in a manner that faithfully represents the *in vivo* function and allows monitoring of a stably trapped mixed disulfide intermediate[28,30]. Mia40 formed DTT-sensitive mixed disulfide intermediates with both yeast Tim10 (a CX_3C substrate) and COX17 (a CX_9C substrate) (**Fig. 7d**, arrowhead). In contrast, the CPS, SPC and SPS Mia40 mutants showed marked differences in their ability to form the mixed disulfide intermediate. The CPS mutant showed a far stronger defect than the SPC mutant, and the double SPS mutant was essentially incapable of forming the intermediate at all (**Fig. 7d**). This agrees well with the complementation data (**Fig. 7c**), is in line with the positioning of Cys55 adjacent to the putative substrate binding hydrophobic cleft in the structure of MIA40 (**Fig. 5**) and supports the concept that Cys55 is the key residue for the reaction with the substrate.

The effect of the mutations is identical for both types of substrate (CX_3C and CX_9C), suggesting that the CPC motif–mediated Mia40 mechanism of oxidation proceeds unaffected by the spacing between the substrate cysteines. The stable covalent mixed disulfide intermediate, obtained in this assay, was found to be consistent with a 1:1 complex of Mia40–Tim10, as shown by blue native PAGE (**Fig. 7e**). This is in agreement with our data in **Supplementary Figure 1** and **Figure 6b**, and shows that monomeric Mia40 is active. The binding assay was also done using immobilized MIA40—the same protein used in all our NMR analyses—to further ascertain that the human and yeast proteins are functionally equivalent. MIA40 can indeed efficiently bind both substrates (CX_9C COX17 and CX_3C yTim10), efficiently and can with either of them form a DTT-sensitive mixed disulfide intermediate, mirroring the behavior of Mia40 (**Supplementary Fig. 5** online).

A final result regards the hydrophobic cleft of MIA40 (**Fig. 7f–h**). When six or eight hydrophobic residues are mutated to alanine, we observed a strong defect *in vitro*, similar to that of the SPS mutant, whereas mutagenesis of only four residues did not result in substantial defects. Retention of binding in two of the three sextuple mutants indicates also that Ile49 and Trp51 are probably less important than the combined effect of Leu56, Met59, Phe72, Phe75, Phe91 and Met94. The fact that several hydrophobic residues must be mutagenized in combination to produce a substantial effect reflects the weak nature of the intermolecular noncovalent hydrophobic interactions, which becomes physiologically relevant when an extended hydrophobic surface is created. Additionally, these interactions are expected to be transient, as more permanent interactions would 'freeze' the intermediate, thus hindering product release from Mia40. As shown by complementation assays (**Fig. 7h**), the cells harboring any of the

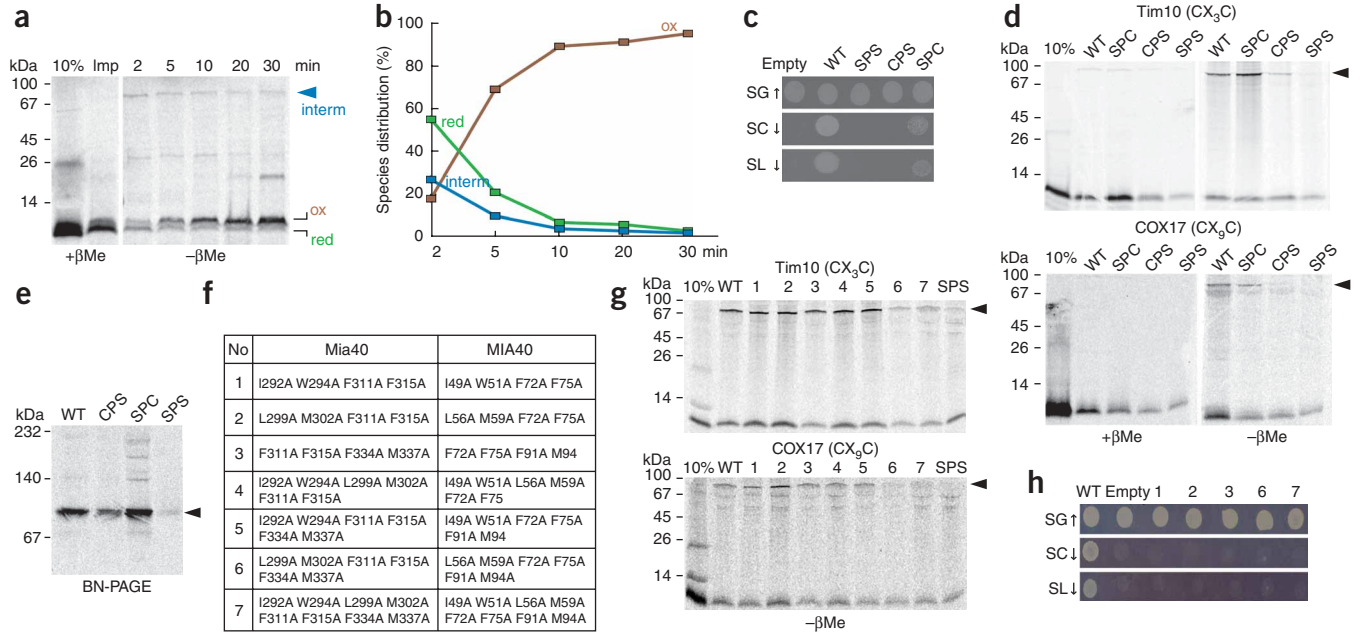

Figure 7 The second cysteine, Cys55, of the active-site CPC is essential *in vivo* and *in vitro*. (**a**) COX17 forms a transient mixed disulfide intermediate with yeast Mia40 *in organello*. ^{35}S-labeled COX17 was imported into wild-type yeast mitochondria for the indicated time points at 30 °C, followed by nonreducing SDS-PAGE and autoradiography. The mixed intermediate ('interm', blue), the oxidized COX17 monomer ('ox', brown) and the reduced COX17 monomer ('red', green) are indicated. (**b**) Quantitative analysis of **a**. The amount of oxidized COX17 increases with time (brown) to the detriment of the transient mixed intermediate with Mia40 (blue) and the reduced COX17 (green). (**c**) *In vivo* complementation of CPC *mia40* mutants. A *GAL-MIA40* strain containing the *MIA40* gene under the control of the *GAL10* promoter was transformed with plasmids carrying wild-type (WT) or cysteine mutants of yeast *MIA40* or nothing (Empty). The resulting transformants were grown in galactose and then shifted to glucose for 18 h before plating on galactose (SG), on glucose (SC) or on lactate with 0.2% (w/v) glucose (SL). (**d**) Reconstitution of binding *in vitro*. Bead-immobilized yeast Mia40 (WT or cysteine mutants) was incubated with radioactive yeast Tim10 (above) or COX17 (below), the interaction was arrested by NEM and protein samples were analyzed by SDS-PAGE (with or without β-mercaptoethanol, +/−βME) and autoradiography. (**e**) The Mia40–Tim10 mixed disulfide intermediate is a 1:1 monomer. ^{35}S-labeled Tim10 was incubated with bead-immobilized Mia40 as in **d**, but the bound material was released from the beads by thrombin and analyzed on blue native PAGE. (**f**) Table showing the mutants that were made in the hydrophobic cleft of yeast Mia40 and the corresponding mutation in MIA40. All of the residues were exchanged with alanines. The same mutant numbering is used in **g** and **h**. (**g**) Reconstitution of binding *in vitro* using the hydrophobic mutants of Mia40, as in **d**. (**h**) *In vivo* complementation of the hydrophobic mutants of Mia40 in the GAL-*MIA40* strain, as in **c**.

mutations in the Mia40 hydrophobic cleft do not survive. This clearly argues for a crucial role of the hydrophobic cleft *in vivo*. A corresponding hydrophobic patch consisting of conserved residues of the substrate is present in helix α_2 of COX17 (**Supplementary Fig. 6** online). We have generated a hypothetical docking model of the COX17–MIA40 adduct, showing the relevant hydrophobic intermolecular interactions, using the program HADDOCK[35] (**Supplementary Fig. 6** and **Supplementary Methods**).

Collectively, the *in vitro* and *in vivo* experiments show that (i) the CPC motif is crucial for the Mia40 oxidative function, (ii) the second cysteine of the CPC motif is the vital active site cysteine, (iii) the hydrophobic cleft mediates substrate binding and (iv) defects observed *in vitro* are mirrored as phenotypes *in vivo*.

DISCUSSION

The structure of MIA40 bears no similarity with any other known oxidoreductase in the cell, thus defining MIA40 as a new type of oxidoreductase. It does not have a thioredoxin domain, which is common among other known oxidoreductases such as eukaryotic PDI and bacterial Dsb proteins. In fact, the well-folded part of MIA40 is much smaller (66 residues) than the typical thioredoxin domain (about 127 residues). In this respect, MIA40 can be thought of as the most 'minimal' oxidoreductase domain described so far.

MIA40 has an α-hairpin core, common to other mitochondrial proteins that contain CX_9C motifs[36] and are, presumably all, substrates for MIA40. In this respect, MIA40 resembles structurally its own substrates, and they may have evolved from a common ancestor. Functional and structural diversification from a putative common ancestor stems, at least partially, from distinct differences in the N-terminal region upstream of the α-hairpin core. First, the N-terminal lid of MIA40 has a much more defined conformation and is more structurally organized and rigid than the N-terminal end of $COX17_{2S\text{-}S}$. Second, the CPC active site of MIA40, which precedes the well-defined helix α1, lies at a greater distance from the core compared to the CC metal binding motif in $COX17_{2S\text{-}S}$. Third, the N-terminal lid of MIA40 is stabilized onto the core by an extensive array of hydrophobic interactions that are unique to MIA40 and absent in other mitochondrial proteins that share the α-hairpin core. These unique properties of the N-terminal lid endow MIA40 with an oxidoreductase function but not with a copper-chaperone function, in contrast with the equivalent N terminus of COX17.

The N-terminal lid is the functional site of the molecule, with the CPC motif forming the active center. This MIA40-unique motif is accessible to the solvent and positioned favorably for a direct and facile transfer of the disulfide bond to the substrate. In this respect, the CPC motif functions as a redox active site, shuttling between the oxidized and reduced states upon binding to the substrate, without affecting the

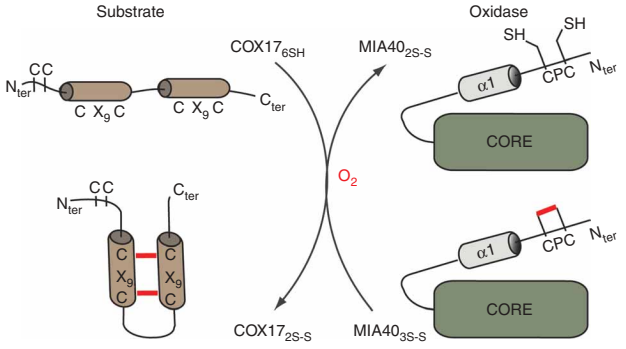

Figure 8 Model for the interaction of MIA40 with its substrates. Schematic representation of the oxidative folding reaction between MIA40$_{3S-S}$ and COX17$_{6SH}$, as observed *in vitro* by NMR. The disulfide bond of the MIA40 CPC redox active site (red) is readily reduced and transferred to the substrate; the second intramolecular disulfide of the substrate can then be formed by O_2. The oxidizing equivalents transferred in the reaction are shown in red.

rest of the MIA40 molecule structurally (**Figs. 3** and **6**). Actually, the CPC motif protrudes into the solvent from a hydrophobic protein surface formed by a number of hydrophobic and aromatic residues, all of which are strictly conserved. The presence of a proline residue in the active site near the hydrophobic cleft where the substrate could bind is a feature of other oxidoreductases such as DsbA and PDI[37,38], and it would be tempting to speculate that it has a functional role. However, mutation of this conserved proline resulted in no apparent changes in mixed disulfide formation with the substrate, nor did it cause growth defects *in vivo* (data not shown). This observation, along with the fact that the crucial proline (for example Pro151 in DsbA, which is adjacent to the active site CPHC motif at residues 30–33 of DsbA) is in a *cis* conformation in these other enzymes as opposed to its *trans* conformation in MIA40, argue for a very different mechanism in the case of MIA40 compared to the thioredoxin-like oxidoreductases.

The structural properties of MIA40 may also rationalize the dual function that this protein must perform in the IMS, as an oxidase and as an import receptor: (i) its N-terminal lid is endowed with the oxidation-active CPC site, which introduces disulfides into the substrates, and (ii) the characteristic hydrophobic cleft functions as a substrate recognition and binding site, stabilizing initial noncovalent interactions that appropriately position the partially folded substrates (which usually have exposed hydrophobic segments) so that the first crucial mixed disulfide can form. In this manner, MIA40 fulfills an import-receptor role.

Given these properties of MIA40, and the fact that there is no evidence of a protein disulfide-isomerase activity in the intermembrane space, it seems possible that such an isomerase activity might be dispensable. In agreement with this, MIA40 has a much greater specificity than proteins such as PDI and DsbA and introduces specific disulfide bonds into partially folded substrates that are properly positioned on MIA40. This is the first example of such a protein and distinguishes the oxidative folding pathway from those in the ER of eukaryotes and the periplasm of bacteria.

MIA40 is necessary and sufficient for oxidation of its substrates, via the N-terminal lid CPC motif as its active site, with the second cysteine, Cys55, in CPC being the catalytic residue. The standard redox potential of the CPC disulfide bond (−200 mV) makes oxidation of substrate motifs with more reducing redox potentials, such as −340 mV (CX_9C of COX17) or −320 mV (CX_3C of small Tims), thermodynamically favored. In the same way, oxidation of the CPC itself by the more oxidizing C-terminal CX_2C pair of Erv1 (redox potential of −150 mV) is also favored. The concept of disulfide relay between Erv1, MIA40 and the substrate can be rationalized on the basis of our structural characterization and is in complete agreement with the recent biochemical and reconstitution analysis of the relay system for the yeast proteins[33].

The working model of the electron-transfer reaction that we propose is shown in **Figure 8**: (i) the substrate (for example COX17) in the fully reduced state cannot efficiently be transformed into the partially oxidized state by oxygen alone for kinetic reasons; (ii) MIA40 efficiently favors the formation of one of the two disulfide bonds within the twin CX_9C motif of COX17; (iii) once the first disulfide bond (between Cys35 and Cys44) is introduced by MIA40, the second disulfide bond between the two remaining cysteines of COX17, which are now favorably positioned, can then be formed rapidly by oxygen. *In vivo*, the second disulfide may alternatively be formed by Erv1, which has been found to be physically linked to Mia40 under certain conditions[9]. The ability of MIA40 to catalyze disulfide-bond formation for both CX_9C and CX_3C proteins, as observed for both Cox17 and Tim10, can be rationalized on the following basis: it is sufficient that MIA40 interacts with one cysteine pair, and once this first disulfide bond is formed, the other cysteine pair can undergo a facile oxidation independently of how many residues are in between the two cysteine pairs. Spacing of *n* residues within the CX_nC motifs is crucial for the final stabilization of the substrate structure, either in a relatively aligned two-helical arrangement, as in Cox17 (ref. 36), or when the two helices are more tilted in relation to each other, as it is the case for the small Tims[31]. This working model is consistent with the observation that the fourth cysteine of the CX_3C motif of Tim10 (connected to the first one to form the outer disulfide) is necessary and sufficient (*in vitro* and *in organello)* for release from MIA40 (ref. 30).

In conclusion, here we have elucidated the Mia40-dependent oxidative folding reaction for mitochondrial cysteine-rich proteins at the molecular level. The mechanism, proposed on the basis of *in vitro* and *in vivo* protein-protein interaction studies between Mia40 and its substrates, gives a clear picture of the mitochondrial IMS protein oxidative folding and can explain the wide range of different substrates of Mia40—proteins with repetitive cysteines organized in twin CX_3C (small Tims), twin CX_9C (Cox17, Cox19, Mdm35, Mic14, Mic17) or twin CX_2C motifs (Erv1). The present results are an important step toward revealing the full molecular details of oxidative protein folding in eukaryotes and the interactions of the mitochondrial machinery dedicated to this process.

METHODS

NMR spectroscopy. We carried out all NMR experiments used for resonance assignment and structure calculations on 0.5–1 mM ^{13}C,^{15}N-labeled and ^{15}N-labeled MIA40$_{2S-S}$ and MIA40$_{3S-S}$ samples in 50 mM phosphate buffer, pH 7.0, containing 10% (v/v) D_2O (plus 2 mM DTT for MIA40$_{2S-S}$). All NMR spectra were collected at 298 K, processed using the standard Bruker software (Topspin) and analyzed through the CARA program[39]. The ^1H, ^{13}C and ^{15}N resonance assignments of MIA40$_{2S-S}$ and MIA40$_{3S-S}$ were performed following a standard protocol using, for backbone assignment, triple-resonance NMR experiments and, for side chain assignment, TOCSY-based NMR experiments.

Structure calculations of MIA40$_{2S-S}$ were performed with the software package ATNOS/CANDID/CYANA[40–42], using as input the amino acid sequence, the chemical shift lists, three [^1H,^1H]-NOE experiments (two-dimensional NOESY, three-dimensional ^{13}C-resolved NOESY and three-dimensional ^{15}N-resolved NOESY) and ϕ and ψ dihedral angle constraints

Table 1 NMR and refinement statistics for $MIA40_{2S\text{-}S}$

	$MIA40_{2S\text{-}S}$
NMR distance and dihedral constraints	
Distance constraints	
Total NOE	1,321
Intra-residue	230
Inter-residue	1,091
Sequential ($\|i-j\|=1$)	437
Medium-range ($\|i-j\|<4$)	398
Long-range ($\|i-j\|>5$)	256
Hydrogen bonds	18
Total dihedral angle restraints	60
ϕ	30
ψ	30
Structure statistics	
Violations (mean ± s.d.)	
Distance constraints (Å)	0.018 ± 0.001
Dihedral angle constraints (°)	0.48 ± 0.18
Max. dihedral angle violation (°)	1.65 ± 0.38
Max. distance constraint violation (Å)	0.33 ± 0.03
Deviations from idealized geometry	
Bond lengths (Å)	0.0214 ± 0.0001
Bond angles (°)	2.574 ± 0.057
Impropers (°)	6.685 ± 0.595
Average pairwise r.m.s. deviation* (Å)	
Heavy	0.51 ± 0.12
Backbone	0.90 ± 0.09

*Pairwise r.m.s. deviation was calculated among 20 refined structures.

derived from the chemical shift index analysis[34]. CSI and PECAN software[43] were used to estimate protein secondary structure. In addition, two disulfide bonds between Cys64 and Cys97 and between Cys74 and Cys87 were imposed, as resulted from their ^{13}C chemical shift analysis. All the other possible combinations of disulfide pairing determine a drastic increase in CYANA target function, as they are not in agreement with long-range NOE patterns.

We subjected the 20 conformers with the lowest residual target function values to restrained energy minimization in explicit water with AMBER 8.0 (ref. 44) and evaluated the quality of the structures with the programs PROCHECK, PROCHECK-NMR[45] and WHATIF[46]. The conformational and energetic analyses of the final REM family of 20 structures are reported in **Table 1**. The Ramachandran plot of the mean minimized structure of $MIA40_{2S\text{-}S}$ shows that 81.1% of residues lie in the most favorable region of the plot, 18.9% of residues lie in the allowed region and no residues lie in the generously and disallowed regions.

We performed relaxation experiments on ^{15}N-labeled samples at 500 MHz and 600 MHz, and measured the ^{15}N backbone longitudinal (R_1) and transverse (R_2) relaxation rates, as well as the heteronuclear $^{15}N\{^1H\}$ NOEs, as previously described[47,48].

We followed disulfide reduction of the $MIA40_{3S\text{-}S}$ form by NMR. Up to 100 mM DTT was added stepwise in anaerobic conditions to ^{15}N-labeled $MIA40_{3S\text{-}S}$ in 50 mM phosphate buffer, pH 7.0, containing 10% (v/v) D_2O, and we acquired two-dimensional ^1H-^{15}N HSQC spectra.

To follow the oxidative folding of COX17, we first produced ^{15}N-labeled or ^{15}N, ^{13}C-labeled $COX17_{6SH}$, adding a large excess of DTT, which was then removed through a PD-10 desalting column, and the cysteine redox state was then checked by NMR. $COX17_{6SH}$ was then left at air exposure or was titrated with ^{15}N-labeled $MIA40_{3S\text{-}S}$ at 25 °C, following the reaction by two-dimensional ^1H-^{15}N HSQC spectra and/or triple-resonance experiments. We followed a similar procedure for the reaction between (^{13}C,^{15}N)cysteine-selectively labeled $COX17_{6SH}$ mutants and unlabeled $Mia40_{3S\text{-}S}$.

Import in yeast mitochondria. We synthesized ^{35}S-labeled precursor proteins using the TNT SP6 coupled transcription/translation kit (Promega). We imported the radioactive material in wild-type yeast mitochondria (50–100 μg) in the presence of 2 mM ATP and 2.5 mM NADH for the indicated time points at 30 °C. We then resuspended mitochondria in 1.2 M sorbitol and 20 mM HEPES, pH 7.4, followed by a treatment with proteinase K (0.1 mg ml^{-1}) to remove unimported material and resuspension in Laemmli sample buffer with or without β-mercaptoethanol, as indicated. We analyzed samples by SDS-PAGE and digital autoradiography (Molecular Dynamics). For the competition experiments, we imported the radioactive precursors in mitochondria with or without 10 μM of recombinant MIA40.

***In vitro* reconstitution of substrate binding on Mia40.** We immobilized Mia40 as a GST-fusion and incubated it with radioactive precursor for 10 min at 4 °C. The reaction was stopped with the addition of 10 mM *N*-ethylmaleimide. We then washed the bound material three times with 150 mM NaCl, 50 mM Tris, pH 7.4, 0.1% (w/v) BSA and 0.1% (v/v) Triton X-100, resuspended it in Laemmli buffer and analyzed it by nonreducing SDS-PAGE and autoradiography (Molecular Dynamics). For the blue native analysis, we released the bound material from the beads by thrombin treatment for 1 h at 4 °C. The released fraction was then loaded onto a 6–16% (v/v) gradient blue native electrophoresis gel[49] followed by autoradiography.

Accession codes. Protein Data Bank: The atomic coordinates and structural restraints for $MIA40_{2S\text{-}S}$ have been deposited under accession code 2K3J. BioMagResBank: resonance assignments are under accession code 15763.

Note: Supplementary information is available on the Nature Structural & Molecular Biology website.

ACKNOWLEDGMENTS

We are grateful to A. Makris (Mediterranean Agronomic Institute of Chania, Crete) for the plasmid M4801, N. Pfanner (University of Freiburg) for the porin SP6 plasmid, N. Petrakis (K.T. laboratory, Institute of Molecular Biology and Biotechnology-Foundation for Research and Technology (IMBB-FORTH)) for help with the use of the Chimera software used in **Figure 5**, A. Hatzi (K.T. group, IMBB-FORTH) for some help with part of the mutagenesis and T. Economou (IMBB-FORTH) and T. Pugsley (Institut Pasteur) for comments on the manuscript. This work was supported by European Network of Research Infrastructures for Providing Access and Technological Advancements in Bio-NMR Contract 026145, by the SPINE II-COMPLEXES Contract, LSHG-CT-2006-031220 "From Receptor to Gene: Structures of Complexes from Signalling Pathways Linking Immunology, Neurobiology and Cancer," and by funds from IMBB-FORTH, the University of Crete and the European Social Fund and National Resources (to K.T.). D.P.S. was supported by a PENED grant. This work was also supported in part by the Italian MIUR-FIRB (Fondo per gli Investimenti della Ricerca di Base, Grant protocollo, MIUR-RBLA032ZM7). Molecular graphics images were produced using the UCSF Chimera package[50] from the Resource for Biocomputing, Visualization, and Informatics at the University of California, San Francisco (supported by the US National Institutes of Health grant P41 RR-01081).

AUTHOR CONTRIBUTIONS

I.B. and L.B. planned the research, discussed and guided the flow of experiments and coordinated the writing of the text, to which all the co-authors contributed; M.M. and C.C. coordinated and performed protein production and characterization; A.G. solved the $MIA40_{2S\text{-}S}$ NMR structure; S.C.-B. planned and recorded the NMR spectra and coordinated the titration experiments; D.P.S. performed the *in vivo* and *in vitro* mutational analysis and interactions and analyzed data; N.K. provided technical support; K.T. designed experiments, analyzed data and coordinated the presentation of the data and the writing of the paper.

Published online at http://www.nature.com/nsmb/
Reprints and permissions information is available online at http://npg.nature.com/reprintsandpermissions/

1. Gruber, C.W., Cemazar, M., Heras, B., Martin, J.L. & Craik, D.J. Protein disulphide isomerase: the structure of oxidative folding. *Trends Biochem. Sci.* **31**, 455–464 (2006).
2. Hatahet, F. & Ruddock, L.W. Substrate recognition by the protein disulfide isomerases. *FEBS J.* **274**, 5223–5234 (2007).
3. Sevier, C.S. & Kaiser, C.A. Ero1 and redox homeostasis in the endoplasmic reticulum. *Biochim. Biophys. Acta* **1783**, 549–556 (2008).

4. Collet, J.F. & Bardwell, J.C. Oxidative protein folding in bacteria. *Mol. Microbiol.* **44**, 1–8 (2002).
5. Kadokura, H., Katzen, F. & Beckwith, J. Protein disulfide bond formation in prokaryotes. *Annu. Rev. Biochem.* **72**, 111–135 (2003).
6. Nakamoto, H. & Bardwell, J.C. Catalysis of disulfide bond formation and isomerization in the *Escherichia coli* periplasm. *Biochim. Biophys. Acta* **1694**, 111–119 (2004).
7. Chacinska, A. *et al.* Essential role of Mia40 in import and assembly of mitochondrial intermembrane space proteins. *EMBO J.* **23**, 3735–3746 (2004).
8. Lu, H., Allen, S., Wardleworth, L., Savory, P. & Tokatlidis, K. Functional TIM10 chaperone assembly is redox-regulated *in vivo*. *J. Biol. Chem.* **279**, 18952–18958 (2004).
9. Mesecke, N. *et al.* A disulfide relay system in the intermembrane space of mitochondria that mediates protein import. *Cell* **121**, 1059–1069 (2005).
10. Tokatlidis, K. A disulfide relay system in mitochondria. *Cell* **121**, 965–967 (2005).
11. Allen, S., Balabanidou, V., Sideris, D.P., Lisowsky, T. & Tokatlidis, K. Erv1 mediates the Mia40-dependent protein import pathway and provides a functional link to the respiratory chain by shuttling electrons to cytochrome *c*. *J. Mol. Biol.* **353**, 937–944 (2005).
12. Bihlmaier, K. *et al.* The disulfide relay system of mitochondria is connected to the respiratory chain. *J. Cell Biol.* **179**, 389–395 (2007).
13. Dabir, D.V. *et al.* A role for cytochrome *c* and cytochrome *c* peroxidase in electron shuttling from Erv1. *EMBO J.* **26**, 4801–4811 (2007).
14. Rissler, M. *et al.* The essential mitochondrial protein Erv1 cooperates with Mia40 in biogenesis of intermembrane space proteins. *J. Mol. Biol.* **353**, 485–492 (2005).
15. Naoe, M. *et al.* Identification of Tim40 that mediates protein sorting to the mitochondrial intermembrane space. *J. Biol. Chem.* **279**, 47815–47821 (2004).
16. Terziyska, N. *et al.* Mia40, a novel factor for protein import into the intermembrane space of mitochondria is able to bind metal ions. *FEBS Lett.* **579**, 179–184 (2005).
17. Hofmann, S. *et al.* Functional and mutational characterization of human MIA40 acting during import into the mitochondrial intermembrane space. *J. Mol. Biol.* **353**, 517–528 (2005).
18. Gabriel, K. *et al.* Novel mitochondrial intermembrane space proteins as substrates of the MIA import pathway. *J. Mol. Biol.* **365**, 612–620 (2007).
19. Cobine, P.A., Pierrel, F. & Winge, D.R. Copper trafficking to the mitochondrion and assembly of copper metalloenzymes. *Biochim. Biophys. Acta* **1763**, 759–772 (2006).
20. Banci, L. *et al.* Mitochondrial copper(I) transfer from Cox17 to Sco1 is coupled to electron transfer. *Proc. Natl. Acad. Sci. USA* **105**, 6803–6808 (2008).
21. Banci, L. *et al.* Modeling protein-protein complexes involved in the cytochrome *c* oxidase copper-delivery pathway. *J. Proteome Res.* **6**, 1530–1539 (2007).
22. Bauer, M.F., Hofmann, S., Neupert, W. & Brunner, M. Protein translocation into mitochondria: the role of TIM complexes. *Trends Cell Biol.* **10**, 25–31 (2000).
23. Endres, M., Neupert, W. & Brunner, M. Transport of the ADP/ATP carrier of mitochondria from the TOM complex to the TIM22.54 complex. *EMBO J.* **18**, 3214–3221 (1999).
24. Vial, S. *et al.* Assembly of Tim9 and Tim10 into a functional chaperone. *J. Biol. Chem.* **277**, 36100–36108 (2002).
25. Sevier, C.S. & Kaiser, C.A. Conservation and diversity of the cellular disulfide bond formation pathways. *Antioxid. Redox Signal.* **8**, 797–811 (2006).
26. Tu, B.P. & Weissman, J.S. Oxidative protein folding in eukaryotes: mechanisms and consequences. *J. Cell Biol.* **164**, 341–346 (2004).
27. Wilkinson, B. & Gilbert, H.F. Protein disulfide isomerase. *Biochim. Biophys. Acta* **1699**, 35–44 (2004).
28. Milenkovic, D. *et al.* Biogenesis of the essential Tim9-Tim10 chaperone complex of mitochondria: site-specific recognition of cysteine residues by the intermembrane space receptor Mia40. *J. Biol. Chem.* **282**, 22472–22480 (2007).
29. Muller, J.M., Milenkovic, D., Guiard, B., Pfanner, N. & Chacinska, A. Precursor oxidation by Mia40 and Erv1 promotes vectorial transport of proteins into the mitochondrial intermembrane space. *Mol. Biol. Cell* **19**, 226–236 (2008).
30. Sideris, D.P. & Tokatlidis, K. Oxidative folding of small Tims is mediated by site-specific docking onto Mia40 in the mitochondrial intermembrane space. *Mol. Microbiol.* **65**, 1360–1373 (2007).
31. Webb, C.T., Gorman, M.A., Lazarou, M., Ryan, M.T. & Gulbis, J.M. Crystal structure of the mitochondrial chaperone TIM9.10 reveals a six-bladed α-propeller. *Mol. Cell* **21**, 123–133 (2006).
32. Sharma, D. & Rajarathnam, K. ^{13}C NMR chemical shifts can predict disulfide bond formation. *J. Biomol. NMR* **18**, 165–171 (2000).
33. Grumbt, B., Stroobant, V., Terziyska, N., Israel, L. & Hell, K. Functional characterization of Mia40p, the central component of the disulfide relay system of the mitochondrial intermembrane space. *J. Biol. Chem.* **282**, 37461–37470 (2007).
34. Wishart, D.S. & Sykes, B.D. The ^{13}C chemical shift index: a simple method for the identification of protein secondary structure using ^{13}C chemical shift data. *J. Biomol. NMR* **4**, 171–180 (1994).
35. Dominguez, C., Boelens, R. & Bonvin, A.M. HADDOCK: a protein-protein docking approach based on biochemical or biophysical information. *J. Am. Chem. Soc.* **125**, 1731–1737 (2003).
36. Banci, L. *et al.* A structural-dynamical characterization of human Cox17. *J. Biol. Chem.* **283**, 7912–7920 (2008).
37. Kadokura, H., Tian, H., Zander, T., Bardwell, J.C. & Beckwith, J. Snapshots of DsbA in action: detection of proteins in the process of oxidative folding. *Science* **303**, 534–537 (2004).
38. Qin, J., Clore, G.M., Kennedy, W.P., Kuszewski, J. & Gronenborn, A.M. The solution structure of human thioredoxin complexed with its target from Ref-1 reveals peptide chain reversal. *Structure* **4**, 613–620 (1996).
39. Keller, R. The Computer Aided Resonance Assignment Tutorial (Cantina, Goldau, 2004).
40. Guntert, P. Automatd NMR structure calculation with CYANA. *Methods Mol. Biol.* **278**, 353–378 (2004).
41. Herrmann, T., Güntert, P. & Wüthrich, K. Protein NMR structure determination with automated NOE assignment using the new software CANDID and the torsion angle dynamics algorithm DYANA. *J. Mol. Biol.* **319**, 209–227 (2002).
42. Herrmann, T., Güntert, P. & Wüthrich, K. Protein NMR structure determination with automated NOE-identification in the NOESY spectra using the new software ATNOS. *J. Biomol. NMR* **24**, 171–189 (2002).
43. Eghbalnia, H.R., Wang, L., Bahrani, A., Assadi, A. & Markley, J.L. Protein energetic conformational analysis from NMR chemical shifts (PECAN) and its use in determining secondary structural elements. *J. Biomol. NMR* **32**, 71–81 (2005).
44. Case, D.A. *et al.* AMBER 8.0, (San Francisco, CA, University of California 2004).
45. Laskowski, R.A., Rullmann, J.A.C., MacArthur, M.W., Kaptein, R. & Thornton, J.M. AQUA and PROCHECK-NMR: programs for checking the quality of protein structures solved by NMR. *J. Biomol. NMR* **8**, 477–486 (1996).
46. Vriend, G. WHAT IF: a molecular modeling and drug design program. *J. Mol. Graph.* **8**, 52–56 (1990).
47. Farrow, N.A. *et al.* Backbone dynamics of a free and phosphopeptide-complexed Src homology 2 domain studied by ^{15}N NMR relaxation. *Biochemistry* **33**, 5984–6003 (1994).
48. Grzesiek, S. & Bax, A. The importance of not saturating H_2O in protein NMR. Application to sensitivity enhancement and NOE measurements. *J. Am. Chem. Soc.* **115**, 12593–12594 (1993).
49. Schagger, H. & Von Jagow, G. Blue native electrophoresis for isolation of membrane protein complexes in enzymatically active form. *Anal. Biochem.* **199**, 223–231 (1991).
50. Pettersen, E.F. *et al.* UCSF Chimera—a visualization system for exploratory research and analysis. *J. Comput. Chem.* **25**, 1605–1612 (2004).
51. Banci, L. *et al.* Human Sco1 functional studies and pathological implications of the P174L mutant. *Proc. Natl. Acad. Sci. USA* **104**, 15–20 (2007).